SLAC-PUB-2429
LBL-10132
November 1979
(T/E)

RECENT RESULTS FROM THE MARK II DETECTOR AT SPEAR*

SLAC-LBL Collaboration[1]

Presented by Jonathan Dorfan
Stanford Linear Accelerator Center
Stanford University, Stanford, California 94305

ABSTRACT

Recent results from the Mark II Detector at SPEAR are presented. These include measurements of the decays $\tau^- \to \rho^- \nu_\tau$ and $\tau^- \to K^{*-}(890)\nu_\tau$, observation of direct photons at the ψ, inclusive proton and Λ production and measurements of charmed baryon and charmed meson decays.

INTRODUCTION

The Mark II detector was installed in the west interaction region at SPEAR in October 1977. All the major detector systems were operational by March 1978 and since then data were obtained in the center-of-mass energy region 3-7.4 GeV. In particular data were recorded at the $\psi(3096)$, $\psi(3684)$ and $\psi(3770)$ resonances and at 3.52 GeV, 3.67 GeV, 4.16 GeV, 4.4 GeV, 5.2 GeV, 6.5 GeV and 7.4 GeV. The region from 3.7-6 GeV was scanned using a step size of 6-20 MeV recording 100-300 μ-pairs per scan point. A broad range of physics measurements has resulted from these data and a subset of the more recent results are presented herein. A notable exception in this presentation is the first observation of the production of a resonance (η') in two photon physics and a measurement of its radiative width.[2] Topics which are forthcoming include a measurement of the total hadronic cross section, limits on rare decay modes of the heavy lepton and measurements of the cascade and hadronic decays of the χ charmonium states. The Mark II magnetic detector is described below as a preface to the following physics topics:

(1) The decays $\tau^- \to \rho^- \nu_\tau$ and $\tau^- \to K^{*-}(890)\nu_\tau$.

(2) Inclusive photons at the $\psi(3096)$ and evidence for the production of direct photons.

(3) Inclusive proton and Λ^0 production.

(4) Observation of the production of charmed baryons.

(5) The $\psi(3770)$ resonance.

(6) Decays of the charmed D mesons.

---

* Work supported primarily by the Department of Energy under contract numbers DE-AC03-76SF00515 and W-7405-ENG-48.

(Invited talk presented at the Annual Meeting of the American Physical Society, Division of Particle and Fields, McGill University, Montreal, Canada, October 25-27, 1979.)

THE MARK II DETECTOR

The SLAC-LBL Mark II solenoidal magnetic detector is shown in end view in Fig. 1. The design goals were to build a detector which

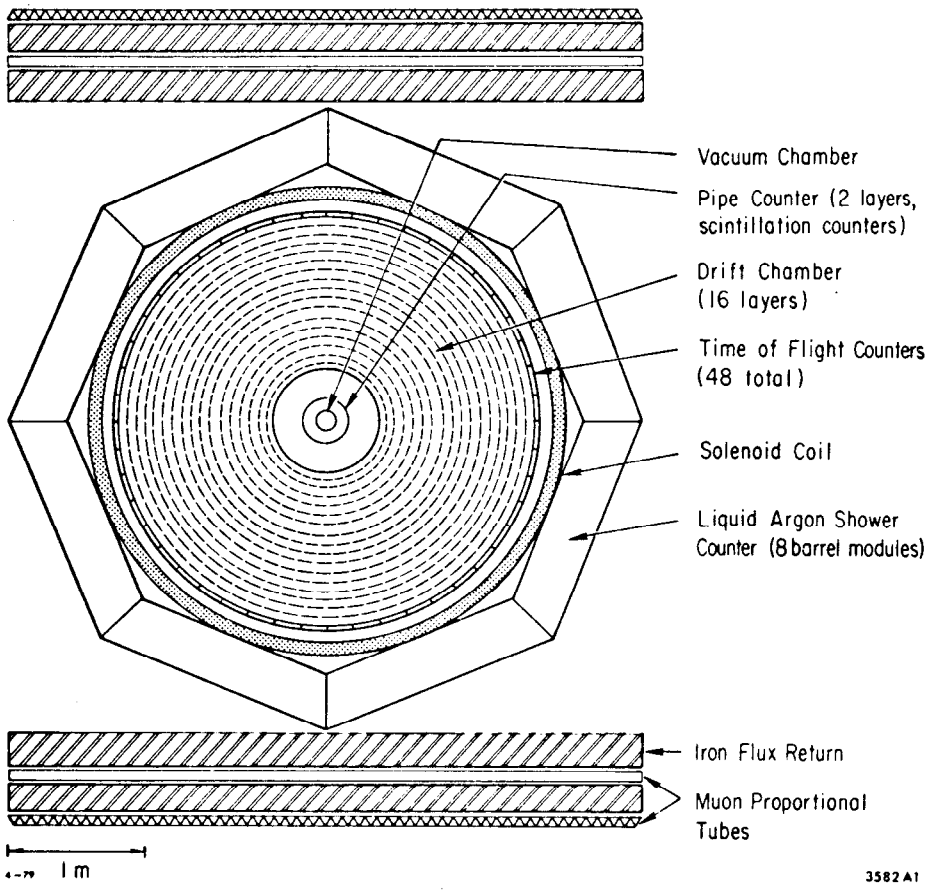

Fig. 1. End view of the SLAC-LBL Mark II detector.

tracked charged and neutral particles with good precision and efficiency over a large solid angle. In addition high priority was given to the identification of leptons with small hadron contamination and the clean separation of pions, kaons and protons over a wide range of momenta. The principal features of the detector are:

(a) Sixteen layers of drift chamber[3] which provide charged particle tracking over a solid angle of 75% of 4π. Azimuthal tracking information comes from 6 axial layers while the remaining 10 stereo layers, strung at $\pm 3^{o}$ to the beam axis, provide polar angle information. The rms momentum resolution for tracks constrained to the $e^{+}e^{-}$ interaction point is $\sigma_p/p = [(0.005p)^2 + (0.0145)^2]^{\frac{1}{2}}$ where p is the track momentum in GeV/c. The two terms in the error parametrization correspond to the measurement error and the multiple scattering respectively. The tracking efficiency is

greater than 95% for tracks whose momenta are above 100 MeV/c.

(b) A time-of-flight (TOF) system comprising 48 scintillation counters arranged azimuthally around the exterior of the drift chamber. This system has a resolution of 300 picoseconds for hadrons which translates into one standard deviation separation levels for momenta of 300 MeV/c for pions and electrons, 1.35 GeV/c for pions and kaons and 2.0 GeV/c for kaons and protons. The following method is used to obtain TOF particle identification for all the physics topics discussed below. The measured momentum and flight path are used to predict a flight time for each mass hypothesis (π, K and proton). A Gaussian weight is obtained for each hypothesis using the difference between the measured and predicted times. These weights, which are proportional to the probability that the measured time is compatable with the mass hypothesis, are summed and normalized to unity. Particles are labeled protons or kaons if their respective weight exceeds 0.5, otherwise the particle is called a pion. A similar scheme is used below 300 MeV/c to label tracks electrons or pions.

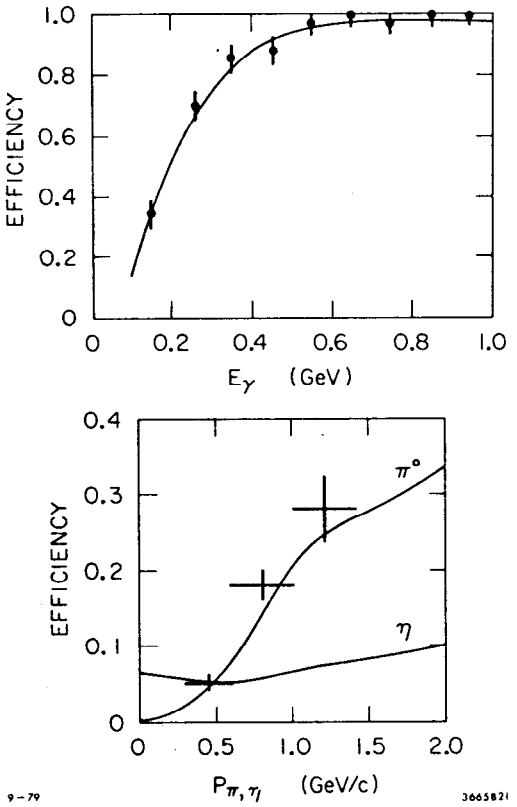

Fig. 2. (a) Photon efficiency for the liquid argon system. (b) π^o and η^o detection efficiency including geometrical effects and $B(\eta \to \gamma\gamma)$. The solid curves are Monte Carlo predictions.

(c) Eight lead-liquid argon shower counters[4] instrumented over 64% of 4π. These counters comprise readout strips parallel, perpendicular and at 45^o to the beam direction and are 14 radiation lengths thick. The energy resolution has been measured to be $\sigma_E/E = 11.5\%/\sqrt{E}$ (E in GeV) for high energy electrons and photons. For energies below 500 MeV this resolution degrades slightly due to the 1.36 rℓ coil which precedes the counters. Angular resolution for high energy photons and electrons has been measured to be 3.5 mrads which in turn degrades to ~8 mrads below 500 MeV. The photon detection efficiency has been measured using the decay $\psi \to \pi^+\pi^-\pi^+\pi^-\pi^o$ and is shown in Fig. 2(a). The solid curve, which is the prediction of the Monte Carlo simulation program,[5] agrees well with the data. Figure 2(b) shows the resulting detection efficiency for π^o and η^o where all geometric effects are included as well as the branching ratio for $\eta^o \to \gamma\gamma$.

(d) Below 300 MeV/c electrons are identified using TOF as described earlier. Above 300 MeV/c cuts in TOF (below 500 MeV/c), total energy, longitudinal and transverse shower development are used to separate electrons and hadrons. The optimal cuts were established from pure samples of electrons, obtained from photon conversions and radiative Bhabhas, and pions obtained from the decay $\psi \to \pi^+\pi^-\pi^+\pi^-\pi^o$. The probability that a hadron is misidentified as an electron has been measured to be 7% below 500 MeV/c, 4% at 600 MeV/c and 2% at 800 MeV/c.

(e) Two layers of proportional tubes interleaved with steel are used for the identification of muons. The threshold momentum for the two layers is 700 MeV/c and 1.0 GeV/c respectively and the system, which covers 55% of 4π, has an efficiency for tagging muons above threshold in excess of 98%. The probability that a hadron is called a muon is 4% at 800 MeV/c, 11% at 900 MeV/c and 2% above 1 GeV/c.

(f) A small angle (25 mrad) tagging system is used to measure Bhabha scattering and hence provides a measure of the luminosity. Large angle Bhabha scattering events are measured in the liquid argon system as a cross-check on this luminosity determination. Typically we assign a 7% systematic error to the measurement of the luminosity.

MEASUREMENT OF THE BRANCHING FRACTIONS FOR $\tau^- \to \rho^-\nu_\tau$ AND $\tau^- \to K^{*-}(890)\nu_\tau$

The heavy lepton, τ^-, is now a well established particle and much is known about its intrinsic properties.[6] There have been many measurements of the leptonic branching fraction as well as the inclusive hadronic branching fractions.[6] The leptonic vertex in τ decays (see Fig. 3) seems to involve the standard V-A Fermi coupling[7] (although V+A has not been entirely ruled out). Inclusive measurements of hadronic final states like (a) $\tau^- \to \pi^-\nu_\tau$, (b) $\tau^- \to \rho^-\nu_\tau$ and (c) $\tau^- \to K^{*-}(890)\nu_\tau$[8] probe the coupling of the weak hadronic current and reactions (a)-(c) have the advantage of separately isolating the strangeness non-changing weak axial vector current, the strangeness non-changing weak vector current and the strangeness changing (i.e., Cabibbo suppressed) weak vector current. The Mark II detector group has measured the branching fractions for all three of these modes and we present below a detailed description of $\tau^- \to \rho^-\nu_\tau$[9] and $\tau^- \to K^{*-}\nu_\tau$ and briefly mention our preliminary result on $\tau^- \to \pi^-\nu_\tau$.

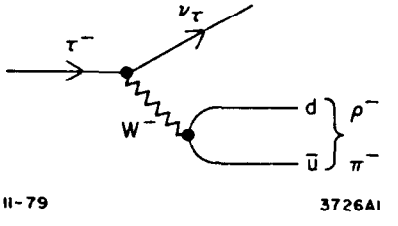

Fig. 3. The hadronic decay of the τ^-.

The data used in the $\tau \to \rho\nu$ study come from a scan in the center-of-mass energy range $4.5 \leq E_{cm} \leq 6.0$ GeV. This corresponds to an integrated luminosity of 3950 nb^{-1} or 11,500 produced $\tau^+\tau^-$ pairs. In searching for the decay $\tau^- \to \rho^-\nu_\tau$ we attempt to isolate events arising from the following decay sequence:

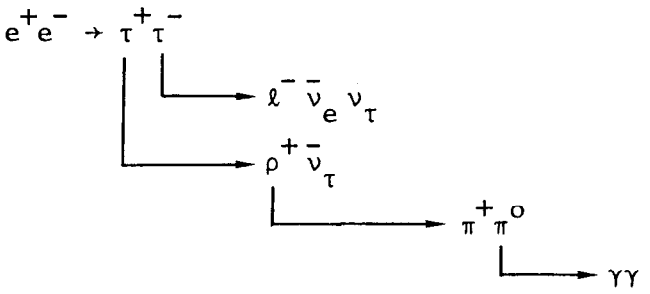

which results in two charged particles and two photons in the detector. Here ℓ^- represents either an electron or a muon and this lepton tag helps provide a clean signature for $\tau^+\tau^-$ pair production. The selected events have two oppositely charged particles, one a pion and the other a lepton, and two photons in the liquid argon shower counters with $E_\gamma \geq 100$ MeV. The two photon invariant mass ($M_{\gamma\gamma}$) spectrum is shown in Fig. 4 and the photon energies for the π^o candidates (those satisfying $80 \leq M_{\gamma\gamma} \leq 200$ MeV/c^2) were adjusted using the π^o mass as a single constraint. These π^o's were then combined with the charged pions to obtain the $\pi^\pm\pi^o$ invariant mass spectrum shown in Fig. 5. The data were fit to the sum of a smooth background and a Breit-Wigner resonance and the ρ mass and width obtained from this fit agree well with the $\rho^\pm$ resonance parameters. There are 85 $\rho^\pm\ell^\mp$ events in the signal region, 64 $\rho^\pm e^\mp$ and 21 $\rho^\pm\mu^\mp$. There are less $\rho\mu$

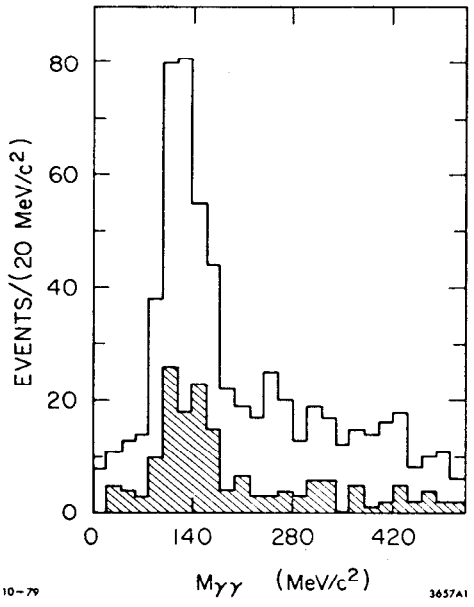

Fig. 4. Two photon invariant mass spectrum for $x^\pm\pi^\mp\gamma\gamma$ events where x represents either a pion or a lepton (ℓ). The shaded distribution is for $\ell^\pm\pi^\mp\gamma\gamma$ events.

events because of the 700 MeV/c momentum threshold of the muon system. The spectrum for the variable $x_\rho = (E_\rho - E_{min})/(E_{max} - E_{min})$, where E_ρ is the measured energy of the ρ and E_{min} and E_{max} are the minimum and maximum energies for a ρ produced in the decay of a τ

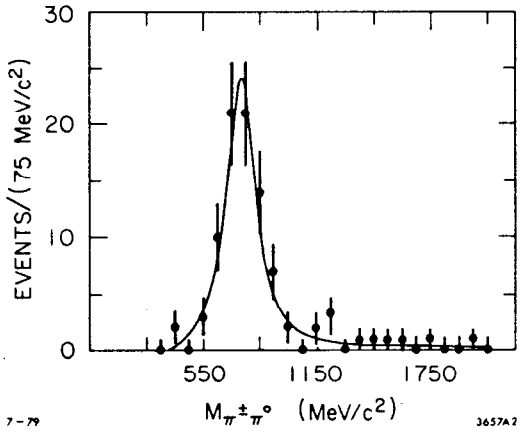

Fig. 5. $\pi^\pm\pi^o$ invariant mass distribution for $\ell^\pm\pi^\mp\pi^o$ events.

at the appropriate center-of-mass energy, is shown in Fig. 6. The data are in good agreement with the Monte Carlo prediction for the two body decay $\tau^- \to \rho^- \nu_\tau$.

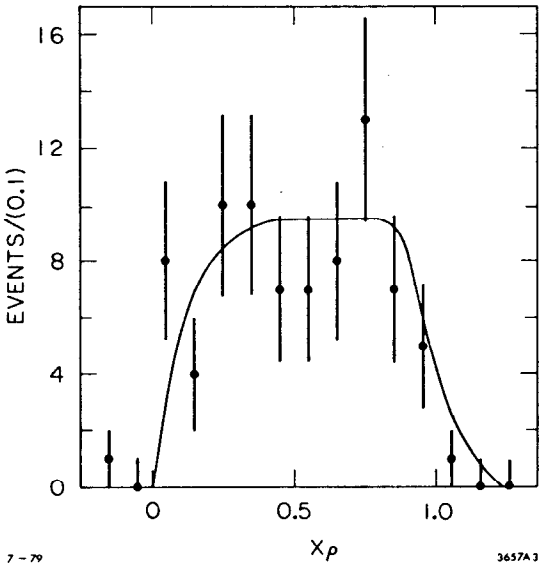

Fig. 6. The distribution $x_\rho = (E_\rho - E_{min})/(E_{max} - E_{min})$ for the 85 $\rho^\pm$ candidates. Here $x_\rho = 0$ (1) corresponds to the minimum (maximum) energy allowed for the ρ in the decay $\tau \to \rho\nu$. The solid line represents the prediction of the Monte Carlo simulation program.

Studies of like-sign events of the type $\rho^\pm \ell^\pm$ indicate that of the 85 events 4 are due to multi-hadron contamination. The remaining 81 events are assumed to be genuine τ decays and we correct for an estimated contribution from $\tau \to A_1 \nu$ and $\tau \to (4\pi)\nu$ of 8.3 ρe events and 2.6 $\rho\mu$ events. In addition we have to correct for a 12.7% loss of events due to spurious photons.

In order to obtain $B(\tau^- \to \rho^- \nu_\tau)$ we need to know $B(\tau^- \to \ell^- \nu_\tau \bar{\nu}_\ell)$. We have used 95 events containing an electron, a muon and no photons to measure the leptonic branching fraction. This channel is background free and the only correction to the data is for the 6% loss of events due to spurious photons.

We have used a Monte Carlo simulation program to obtain the detection efficiencies for the three channels: $\varepsilon_{\rho e} = 6.4\%$, $\varepsilon_{\rho\mu} = 2.7\%$ and $\varepsilon_{e\mu} = 12.9\%$. Combining these with the corrected number of events and the total number of produced $\tau^+\tau^-$ pairs we obtain

$$B(\tau^- \to \rho^- \nu_\tau) B(\tau^+ \to e^+ \bar{\nu}_\tau \nu_e) = 0.042 \pm 0.009$$

$$B(\tau^- \to \rho^- \nu_\tau) B(\tau^+ \to \mu^+ \bar{\nu}_\tau \nu_\mu) = 0.033 \pm 0.010$$

and

$$\sqrt{B(\tau^- \to e^- \nu_\tau \bar{\nu}_e) B(\tau^+ \to \mu^+ \bar{\nu}_\tau \nu_\mu)} = 0.185 \pm 0.015 \quad .$$

The errors quoted are based on the statistics of the uncorrected events and the statistical errors of the corrections and Monte Carlo calculations. In addition systematic errors have been included to account for uncertainties in the luminosity, the lepton tagging efficiencies and misidentifications and radiative corrections for the initial state.

Assuming μ-e universality in τ decays we further obtain

$$B(\tau^- \to \rho^- \nu_\tau) = (20.5 \pm 4.1)\%$$

$$B(\tau^- \to e^- \bar{\nu}_e \nu_\tau) = (18.5 \pm 1.5)\%$$

and

$$\frac{B(\tau^- \to \rho^- \nu_\tau)}{B(\tau^- \to e^- \nu_\tau \bar{\nu}_e)} = 1.11 \pm 0.23 \quad .$$

This ratio can be calculated using the conserved vector current hypothesis and $e^+e^- \to \rho^o$ data. In particular the prediction of Gilman and Miller[10] for this ratio is 1.2 in excellent agreement with the data. The result is also in agreement with the measurement of $B(\tau^- \to \rho^- \nu_\tau) = (24 \pm 9)\%$ of the DASP group.[11] The measurement presented here represents less than 20% of our data and we will soon have a sample of ~500 ρℓ events to upgrade this analysis. We also have obtained a preliminary result of $B(\tau^- \to \pi^- \nu_\tau) = (10.7 \pm 2.1)\%$.

In order to study the decay $\tau^- \to K^{*-}(890)\nu_\tau$ we have used all the Mark II data with $E_{cm} > 4.2$ GeV, which corresponds to an integrated luminosity of 15,300 nb^{-1} or 42,700 produced $\tau^+\tau^-$ pairs. For this analysis we search for one of the following two decay sequences:

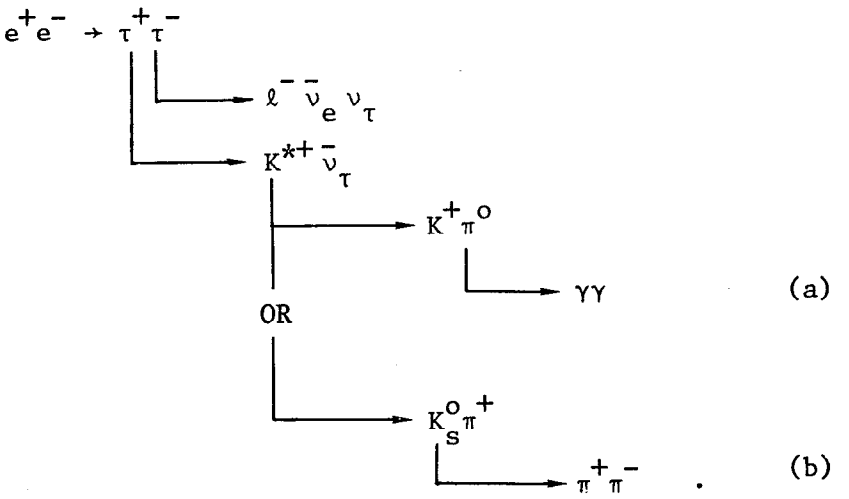

Again the lepton tag is used to isolate the τ channel and we require that the K^* decay either to (a) $K^\pm\pi^o$ or (b) $K^o_S\pi^\pm$. In case (a) the event selection is identical to the ρℓ events except that we require a charged kaon instead of a pion. In case (b) we require that there be four charged tracks with the appropriate charges and that two oppositely charged tracks, both pions, form a secondary vertex (distant from that formed by the $\pi^+\ell^-$ by at least 1 cm) and have a mass consistant with a K^o_S. Figure 7 shows the invariant mass spectrum for the $K^\pm\pi^o$ and $K^o_S\pi^\pm$ events selected as above. A clear peak is seen at the $K^*(890)$. There are 18 signal events with an estimated background of 3.4 events. We have used the detection efficiencies $\varepsilon_{K^+\pi^o\ell^-} = 1.3\%$ and $\varepsilon_{K^o_S\pi^+\ell^-} = 2.4\%$, the number of corrected events

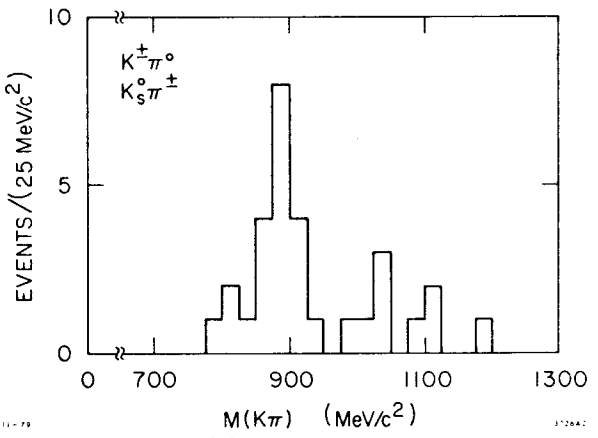

Fig. 7. $K^{\circ}_{S}\pi^{\pm}$ and $K^{\pm}\pi^{\circ}$ invariant mass distribution in candidate events for $\tau^{-} \to K^{*-}(890)\nu_{\tau}$.

and the number of produced $\tau^{+}\tau^{-}$ pairs to obtain

$$B(\tau^{-} \to K^{*-}(890)\nu_{\tau}) =$$

$$1.26 \pm 0.37 \pm 0.32$$

where the first error is statistical and the second error accounts for systematic effects. We interpret this result as evidence for a Cabibbo suppressed decay mode of the τ. Such a mode is expected and according to Tsai[12]

$$\frac{B(\tau \to K^{*}(890)\nu_{\tau})}{B(\tau \to \rho\nu_{\tau})} = \tan^{2}\theta_{c} \cdot f(M_{\tau}, M_{\rho}, M_{K^{*}}).$$

where θ_c is the Cabibbo angle and f (= 0.93) accounts for the difference in phase space available to the two channels. For $\tan^2\theta_c = 0.05$ and $B(\tau \to \rho\nu) = 20.5 \pm 4.1$, theory predicts $B(\tau \to K^{*}(890)\nu_{\tau}) = 1.0 \pm 0.2$ in good agreement with our measurement.

MEASUREMENT OF HIGH ENERGY DIRECT PHOTONS IN ψ DECAYS

First order QCD calculations[13] predict that a significant fraction of the hadronic decays of a heavy quark-antiquark resonance, such as the ψ, should be accompanied by direct photons. A direct photon is defined as one which does not come from π^{o} or η^{o} decay. QCD perceives the hadronic decay of the ψ as going through a 3 gluon intermediate state (see Fig. 8). There is no reason why one of the gluon lines cannot be replaced by a photon in which case hadronic decays of the ψ would contain direct photons. First order QCD predicts

$$B_{\gamma} = \Gamma(\psi \to \gamma gg)/\Gamma(\psi \to ggg) = (\alpha/\alpha_{s})C(e_{Q}/e)^{2}$$

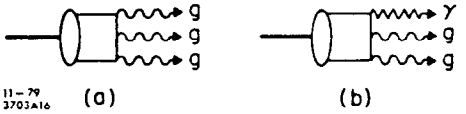

Fig. 8. (a) QCD model for the hadronic decay of the ψ and (b) the contribution to the direct photon production.

where C = 36/5 is a color SU(3) factor, e_Q is the charge of the charmed quark, and α_s is the strong coupling constant. For $\alpha_s = 0.18$,[14] one calculates $B_{\gamma} = 13\%$. If we equate the decay of ψ into hadrons with the 3 gluon decay and correct for second-order electromagnetic effects, the first order QCD prediction for the branching ratio for

direct photons from the ψ is 8%. The photon momentum spectrum is predicted to be roughly linear, peaking at the beam energy.

The data used for this analysis comprises 280,000 hadronic events at the ψ. The events are required to have at least two charged particles and background due to Bhabha events, in which one of the electrons radiates, is removed. Photons are detected in the liquid argon shower counters. Neutral pions are reconstructed by combining pairs of photons each of which is required to have $E_\gamma \geq 150$ MeV. Photon pairs with an invariant mass between 75 and 200 MeV are considered to be π^o candidates and the candidate events are then corrected (as a function of π^o momentum) for background. The shape of the background was obtained by combining real photons with "pseudo-photons" from the same event. Pseudo-photons were created by assigning charged π's a π^o identity and letting them decay into two photons. The background was normalized to the two photon mass spectrum above 300 MeV/c^2.

The photons and π^o's obtained in this way are used to obtain inclusive photon and π^o spectra. The detected spectra are corrected using the known photon and π^o detection efficiencies and the trigger efficiency. The trigger efficiency is obtained from a sample of ψ' decays. Events of the type $\psi' \to \psi\pi^+\pi^-$ are selected which have two oppositely charged particles whose missing mass is consistant with the ψ mass. This sample of ψ events is identified solely by the π^+ and π^- and hence there is no trigger bias associated with the ψ. Trigger efficiencies as a function of photon and π^o momenta are obtained from these events as the fraction of ψ events which would have triggered the Mark II in the absence of the π^+ and π^-. The photon trigger efficiency varies from 70% at $x = 0.1$ to ~40% near $x = 1.0$ where for a photon of momentum p, $x = 2p/M_\psi$. The π^o trigger efficiency varies from 70% at $x = 0.3$ to ~50% at $x = 1.0$.

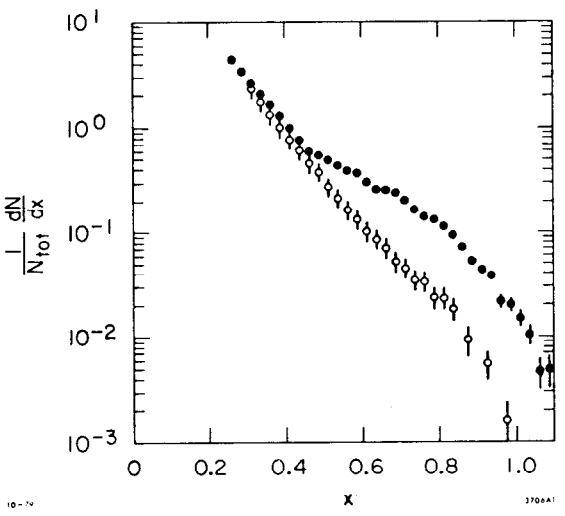

Fig. 9. Solid points show the inclusive photon momentum distribution. Open points show the expected photon momentum distribution based on measurements of π^o and η^o production. The error bars on the measured photons are statistical only; the error bars on the expected distribution include a ±20% systematic error.

The solid points in Fig. 9 show the inclusive photon spectrum after correction for the trigger efficiency and the photon detection efficiency. The distribution has been normalized to the total number of produced ψ's and the error bars are statistical only. Typical systematic errors are ±20%, approximately half of which are x dependent. Fig. 10 shows the π^o inclusive spectrum. Systematic errors of ±30% are not shown.

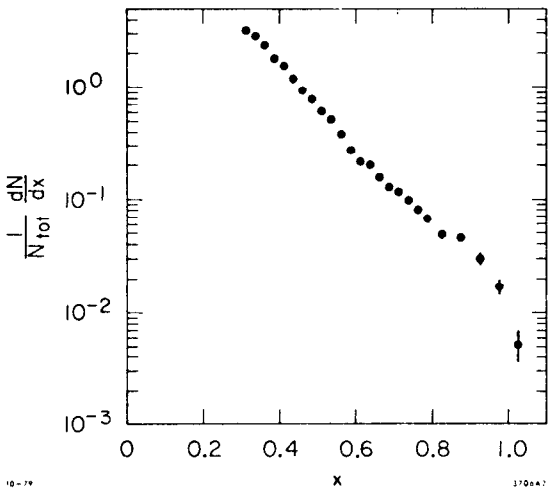

Fig. 10. Inclusive π^o momentum distribution. Systematic error are ±30% and are not shown on the figure.

include a ±22% systematic error. inclusive photons for $x \geq 0.5$.

Figure 11 shows the difference between the two distributions in Fig. 9 and is hence the excess of measured photons over and above those arising from π^o and η^o decays. Both statistical and systematic errors are shown although there is an additional ±17% systematic error in the subtracted distribution due to uncertainties in the efficiency corrections and knowledge of the direct photon angular distribution. Integrating the direct photon momentum distribution above $x = 0.6$ we obtain an inclusive rate for direct photon production of $(4.1 \pm 0.8)\%$. For $x > 0.6$ first order QCD predicts 5% in good agreement with the data. The shape of the direct photon x distribution predicted by first order QCD and convoluted with our detector resolution is shown in Fig. 11. It does not agree well with the observed shape, but it is important to point out that higher order QCD effects could well be comparable to those in first order. The predicted x distribution will also be softened by radiative

We have used the π^o inclusive distribution to make a prediction for the expected photon x distribution. We have also accounted for photons arising from η^o decay. To determine the η^o contribution, fits have been made to the background subtracted two photon mass distributions. We have measured the ratio $R(p) = B(\psi \to \eta^o + x) \cdot B(\eta^o \to \gamma\gamma)/B(\psi \to \pi^o + x)$ as a function of momentum and find that R(p) is less than 0.1 in all momentum bins except $p > 1.2$ GeV where $R(p) = 0.16 \pm 0.06$. Using these estimates of η^o production and the measured π^o x distribution, we produce the expected photon inclusive distribution shown in Fig. 9 as open circles. The error bars In Fig. 9 we see a clear excess of

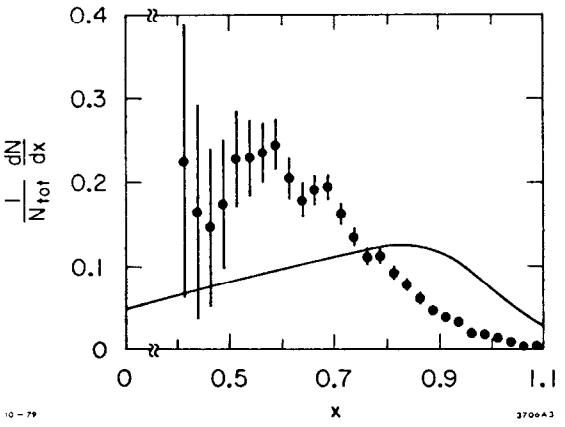

Fig. 11. Direct photon momentum distribution. The solid curve is the lowest order QCD prediction convoluted with the energy resolution.

effects and the mass of the final state hadrons which were not included in the QCD calculations.

The angular distribution for the photons with $x > 0.6$ has been fit to the form $1 + \alpha_\gamma \cos^2\theta$ where θ is the polar angle of the photon with respect to the beam direction. Approximately 25% of these photons are from π^o decay and allowing for an isotropic distribution for these photons we obtain $\alpha_\gamma = 0.18 \pm 0.18$ for the direct photons. First order QCD predicts $\alpha_\gamma \approx 0.3$ for $x > 0.6$.

As a check on possible systematic errors and trigger bias problems, the analysis presented above has been repeated using two other independent methods. The first method uses the ψ events obtained from $\psi' \to \psi\pi^+\pi^-$ as discussed earlier. The second involves using ψ data and requiring one photon in the liquid argon system and another arising from a photon conversion in the 0.06 radiation length of material which precedes the drift chamber. In the first case the π^+ and π^- provide the trigger and in the second the e^+ and e^- from the conversion provide the trigger. So both of these methods are free of the trigger bias, and in both cases the resulting photon and π^o distributions are consistant, within errors, with the primary method discussed above.

INCLUSIVE PROTON AND Λ^o PRODUCTION

A study has been made of the inclusive cross section for the production of protons and Λ^o's in the center-of-mass energy range 3.7-7.4 GeV.[15] A measurement of this nature is important in its own right. However the main motivation for this study was to look for threshold effects which might signify the onset of charmed baryon production.

Anti-protons ($\bar{p}$) were used for this inclusive measurement to avoid the contamination present in proton events from beam-gas scattering. All hadronic events with two or more charged prongs were used for the $\bar{p}$ analysis and TOF was used to identify $\bar{p}$'s with momenta ≤ 2.0 GeV/c. The $\bar{p}$ detection efficiency is estimated from a Monte Carlo model in which $\bar{p}$'s are generated according to the invariant cross section $E/4\pi p^2 d\sigma/dp \sim e^{-bE}$, where p is the momentum of the $\bar{p}$, E its energy and b is an adjustable slope parameter. The rest of the phase space is filled with a second nucleon and $\langle n \rangle - 2$ pions, where $\langle n \rangle$ is the mean particle multiplicity. The parameters b and $\langle n \rangle$ are adjusted at each center-of-mass energy so that the observed $\bar{p}$ momentum spectra are adequately reproduced. As a check on this $\bar{p}$ production model we have used it to obtain invariant cross sections as a function of momentum at various energies in the 4 GeV region and the resulting spectra agree well with those obtained by the DASP group.[16] The detection efficiency for $\bar{p}$'s varies slowly with center-of-mass energy, the average being 60%.

The Λ^o and $\bar{\Lambda}^o$ hyperons are identified by their $p\pi^-$ and $\bar{p}\pi^+$ decay modes. All hadronic events with three or more charged particles were used. The rms mass resolution for the Λ's is 3 MeV and background subtractions of $\lesssim 15\%$ are made. For the Λ's (not $\bar{\Lambda}$'s) we require that the total observed charge be $< +1$. This requirement reduces the beam-gas background substantially and results in an efficiency

of ~75% for Λ's relative to $\bar{\Lambda}$'s. The detection efficiency is obtained from the same Monte Carlo model as the $\bar{p}$'s, and its varies from 10% at 3.7 GeV to 13% at 7.4 GeV.

The results are presented in Fig. 12 in the form of $R(p+\bar{p}) = 2\sigma_{\bar{p}}/\sigma_{\mu\mu}$ and $R(\Lambda+\bar{\Lambda}) = [\sigma_{\Lambda}+\sigma_{\bar{\Lambda}}]/\sigma_{\mu\mu}$ (where $\sigma_{\mu\mu}$ is the μ-pair cross section) as a function of center-of-mass energy. These data have been corrected for acceptance and the Λ branching fraction into $p\pi$. All errors are statistical; the estimated systematic errors are ±17% for $R(p+\bar{p})$ and ±27% for $R(\Lambda+\bar{\Lambda})$ and are dominated by the uncertainties in the production process. It is important to point out that $R(p+\bar{p})$ is not corrected for the contribution of protons from decays of Λ^o or Σ^o hyperons. The measurement of $R(p+\bar{p})$ agrees well in shape but lies ~25% above previous measurements.[16,17] The measurement of $R(\Lambda+\bar{\Lambda})$ is in poor agreement with the previous measurement;[17] the rate measured in the Mark II, which is about 2½ times higher than the previous measurement, is based on a cleaner Λ signal and more detailed efficiency studies. The data for both the $\bar{p}$'s and Λ's show an appreciable increase in baryon yield between 4.6 GeV and 5.2 GeV. The observed step sizes are $\Delta R(p+\bar{p}) = 0.31 \pm 0.06$ and $\Delta R(\Lambda+\bar{\Lambda}) = 0.10 \pm 0.03$ and the Λ/p ratio, corrected for the proton contribution from Λ's, is (41 ± 15)%.

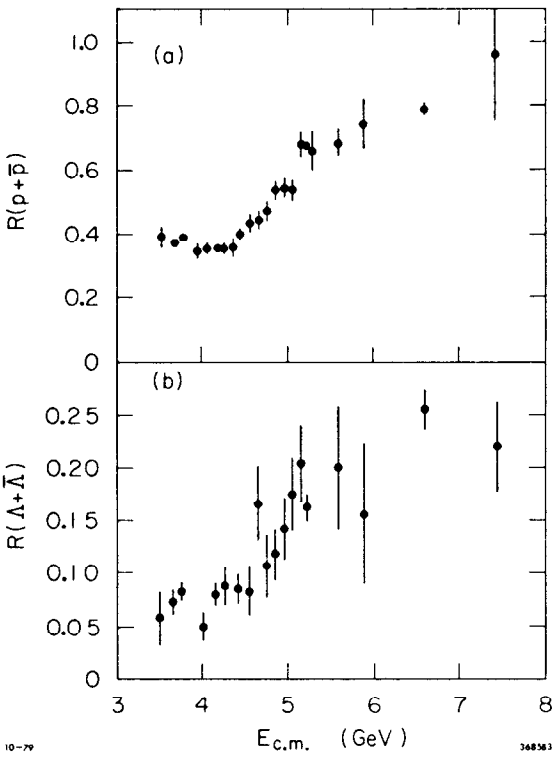

Fig. 12. (a) $R(p+\bar{p})$ as a function of E_{cm} and (b) $R(\Lambda+\bar{\Lambda})$ as a function of E_{cm}. Errors are statistical only.

OBSERVATION OF CHARMED BARYON DECAYS

If the rise in the baryon yield at 4.6 GeV is due to the onset of the production of charmed baryons, exclusive states with masses ~2.3 GeV should be seen decaying into final states containing one unit of baryon number and at least one unit of strangeness. Such weakly decaying states have been sought in invariant mass spectra and a prominent signal has been seen in the channel $pK^-\pi^+ + \bar{p}K^+\pi^-$.[15] All the Mark II data in the center-of-mass energy range 4.5-6.0 GeV are used for the analysis. These data correspond to an integrated luminosity of 9150 nb^{-1}, 5150 nb^{-1} of which is at 5.2 GeV. Charged kaons and protons are identified by the TOF system.

Figure 13 shows the invariant mass for various combinations of pKπ. A recoil mass cut of > 2.2 GeV has been applied to these data. Figure 13(a) shows the invariant mass of $pK^-\pi^+ + \bar{p}K^+\pi^-$ and a narrow signal of 39 ± 8 events is seen at a mass of 2.285 GeV/c^2 above a background of 20 events. The quantum numbers for these two states are those appropriate to the lowest lying charmed baryon, henceforth called Λ_c^+. Figure 13(b) shows the invariant mass of pKπ states whose quantum numbers are not appropriate for the Λ_c^+ and no structure is seen in these channels.

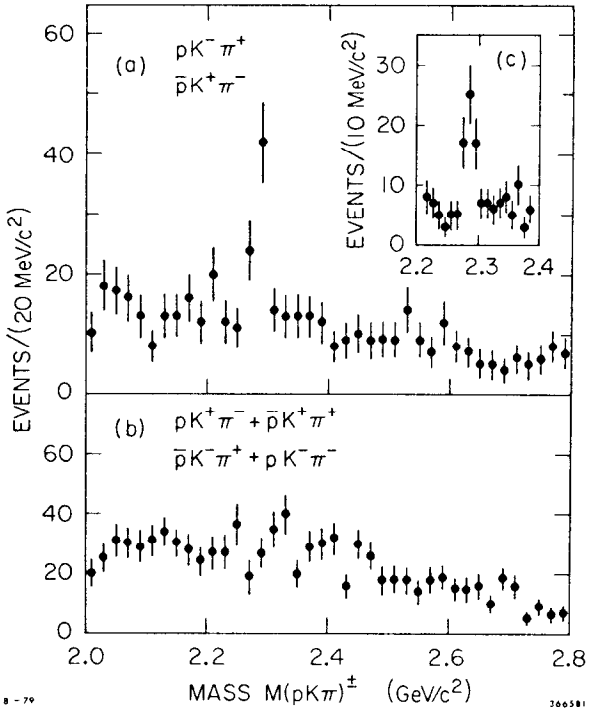

Fig. 13. (a) The combined $pK^-\pi^+$ and $pK^+\pi^-$ invariant mass distribution for recoil masses > 2.2 GeV/c^2. Part of this plot is shown with finer bins in (c). (b) The $pK^+\pi^-$ and $pK^-\pi^-$ (plus charge conjugate states) mass distribution for recoil masses > 2.2 GeV/c^2.

A fit using a Gaussian plus a background shape obtained from Fig. 13(b) has been performed on the data in Fig. 13(a). The width obtained for the Gaussian is consistant with the detector resolution indicating that the pKπ state results from a weak decay. We obtain a mass of 2.285 ± 0.006 GeV/c^2 for the pKπ state, where the error is dominanted by systematic effects. We have also observed a signal in the channel $pK_S^o + \bar{p}K_S^o$ which is shown in Fig. 14. The signal corresponds to 10 ± 5 events and occurs at a mass which is in good agreement with that obtained from the pKπ signal.

A systematic error of 6 MeV/c^2 has been assigned to the mass of the pKπ state. The uncertainty in the magnetic field contributes 2 MeV/c^2 to the mass error. A 20% error in our correction for the proton and antiproton energy loss contributes 2 MeV/c^2. The

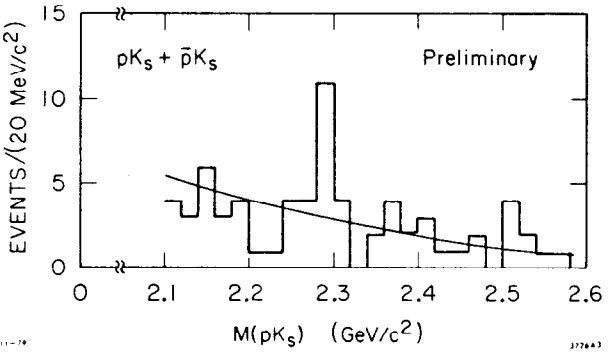

Fig. 14. Invariant mass for pK_S and $\bar{p}K_S$ for events with a recoil mass > 2.2 GeV/c^2.

absolute mass scale is checked using 20,000 reconstructed K^o_s decays whose mass agrees with the world average to within 0.3 MeV/c^2. Furthermore, in data taken many months apart, the D^o mass varies by at most 3 MeV/c^2.

If the observed state is produced in equal mass pairs then the energy of the state will be the beam energy (E_b), and its mass can be calculated as $M = \sqrt{E_b^2 - p^2}$, where p is the momentum of the state. Figure 15 shows this beam constrained mass for the channels $pK^-\pi^+$, pK^o_s and $\Lambda\pi^+$ and their charge conjugates. From the pKπ data in Fig. 15 we find that (26 ± 11)% of the time the pKπ state at 2.285 GeV/c^2 recoils against an equal mass state. From the same data we obtain an independent (i.e., different systematics) measure of the mass of the pKπ state which agrees very well with the determination from the invariant mass plot. Also in Fig. 15 we observe a statistically weak signal in the Λπ mode. An analysis of the pKπ Dalitz plot taking into account the non-resonant contributions leads to resonant contributions of (12 ± 7)% for $K^*(890)$ and (17 ± 7)% for $\Delta^{++}(1236)$.

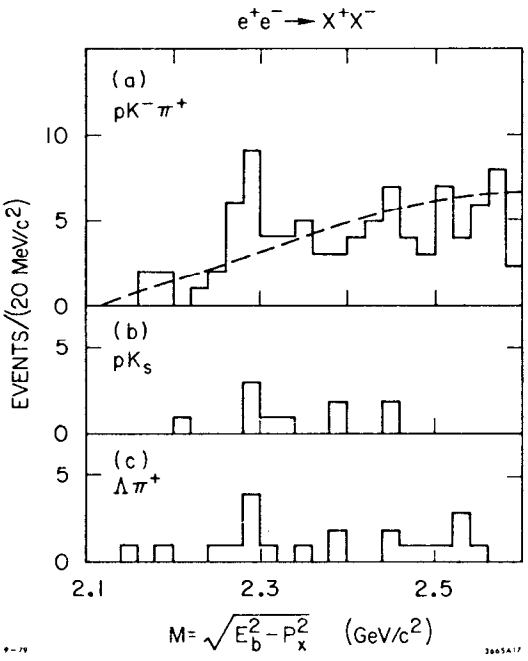

Fig. 15. Beam constrained mass is plotted to search for equal mass production $e^+e^- \to x^+x^-$ where $x^\pm$ decays to (a) $pK^-\pi^+$ or $\bar{p}K^+\pi^-$, (b) pK_s or $\bar{p}K_s$ and (c) $\Lambda\pi^+$ or $\bar{\Lambda}\pi^-$. The dashed curve in (a) represents the estimated background.

The mass, narrow width, quantum numbers of the observed mass combinations and the presence of associated production lead to the most obvious identification of this state as the Λ_c^+. The Λ_c^+ has been observed by several other experiments,[18] although the majority of these experiments have reported a mass near 2.26 GeV/c^2.

A Monte Carlo simulation program has been used to estimate the detection efficiency for the pKπ mode as (13.0 ± 2.5)% which along with the integrated luminosity provides a measure of $\sigma(\Lambda_c + \bar{\Lambda}_c) \cdot B(\Lambda_c \to pK\pi) =$ 0.037 ± 0.012 nb at 5.2 GeV. We have used the measured step size to estimate $\sigma(\Lambda_c + \bar{\Lambda}_c)$ at 5.2 GeV under the following assumptions:

(1) The step ΔR(p) is entirely due to the onset of pair production of charmed baryons.[19]

(2) All charmed baryons so produced cascade down to the Λ_c^+.

(3) The Λ_c^+ decays to a proton (as opposed to a neutron) (60 ± 10)% of the time.[20]

Hence

$$\sigma(\Lambda_c + \bar{\Lambda}_c) = \frac{\Delta R(p+\bar{p})}{0.6}\,\sigma_{\mu\mu}$$

$$= 1.7 \pm 0.4 \text{ nb}$$

and furthermore

$$B(\Lambda_c^+ \to pK^-\pi^+) = (2.2 \pm 1.0)\% \quad .$$

In addition from the 10 $K_s^o p$ events we obtain

$$\frac{B(\Lambda_c^+ \to p\bar{K}^o)}{B(\Lambda_c^+ \to pK^-\pi^+)} = 0.54 \pm 0.25$$

and the 6 $\Lambda\pi$ events in the constrained mass plot (Fig. 15) correspond to

$$\frac{B(\Lambda_c^+ \to \Lambda\pi^+)}{B(\Lambda_c^+ \to pK^-\pi^+)} = 0.35 \pm 0.20 \quad .$$

THE $\psi(3770)$ RESONANCE

The $\psi(3770)$[21,22] resonance lies just above the threshold for the production of D^+D^- and D^oD^o, but below the threshold for DD^* production. It decays entirely to $D\bar{D}$ and provides a sample of kinematically well determined and relatively background-free D mesons. The Mark II group has performed a scan in the energy range 3.67-3.87 GeV in order to measure the $\psi(3770)$ resonance parameters. In addition 2850 nb^{-1} of integrated luminosity were obtained at the fixed energy of 3.771 GeV. The fixed energy running is useful for understanding both inclusive and exclusive properties of the D mesons and absolute branching fractions can be obtained because the scan data provides a measure of the $D\bar{D}$ production cross section.

The scan data is shown in Fig. 16(a) in the form of R which is the ratio of the hadronic cross section to the μ-pair cross section. The contribution from $\tau^+\tau^-$ pairs has been removed and the continuum (but not the ψ, ψ' and ψ'') has been radiatively corrected. The prominant features of Fig. 16(a) are the $\psi(3684)$ and its radiative tail plus a broader resonance centered at ~3.77 GeV, the $\psi(3770)$.

The data in Fig. 16(a) have been fit to a function which accounts for the resonance shape, the continuum and the radiative tails of the $\psi(3096)$, $\psi(3684)$ and the $\psi(3770)$ itself. The form of the resonance shape is a non-relativistic p-wave Breit-Wigner with an energy dependent total width[23] which takes into account the proximity of the resonance to the $D\bar{D}$ threshold. In particular

$$R(E_{cm}) = \frac{1}{\sigma_{\mu\mu}}\,\frac{3\pi}{M^2}\,\frac{\Gamma_{ee}\,\Gamma_{tot}(E_{cm})}{(E_{cm}-M)^2 + \Gamma^2_{tot}(E_{cm})/4}$$

and

$$\Gamma_{tot}(E_{cm}) \propto \frac{p_+^3}{1+(rp_+)^2} + \frac{p_o^3}{1+(rp_o)^2}$$

where p_+ (p_o) is the momentum of the pair produced D^+ (D^o) and the mass of the resonance (M) its total width (Γ_{tot}) and its partial width to electrons (Γ_{ee}) are parameters in the fit. The total width is normalized at the peak of the resonance and the interaction length r is taken to be 2.5 fermis for this analysis. The resonance parameters obtained in the fit are found to be insensitive to the size of r.

The fit has a χ^2 of 12 for 17 degrees of freedom and is shown, after removal of the continuum and radiative effects, superimposed on the data in Fig. 16(b). The parameters obtained from the fit are:

$$M = 3763.7 \pm 5.1 \text{ MeV}/c^2$$
$$\Gamma_{tot} = 23.5 \pm 5.0 \text{ MeV}$$
$$\Gamma_{ee} = 276 \pm 50 \text{ eV} \quad .$$

The errors include systematic effects: the error in the mass is dominated by the 0.13% energy calibration of SPEAR. We also obtain the peak cross section $\sigma(3764) = 9.3 \pm 1.4$ nb.

Table I compares the Mark II results with those of DELCO[22] and the Lead Glass Wall[21] (LGW) experiment. The Mark II measurement of Γ_{tot} agrees well with the previous measurements while Γ_{ee} is intermediate between the two previous measurements. The mass we obtain appears 6-8 MeV/c^2 lower than the previous measurements, which seems to be within errors. However, we can remove the ring calibration error by

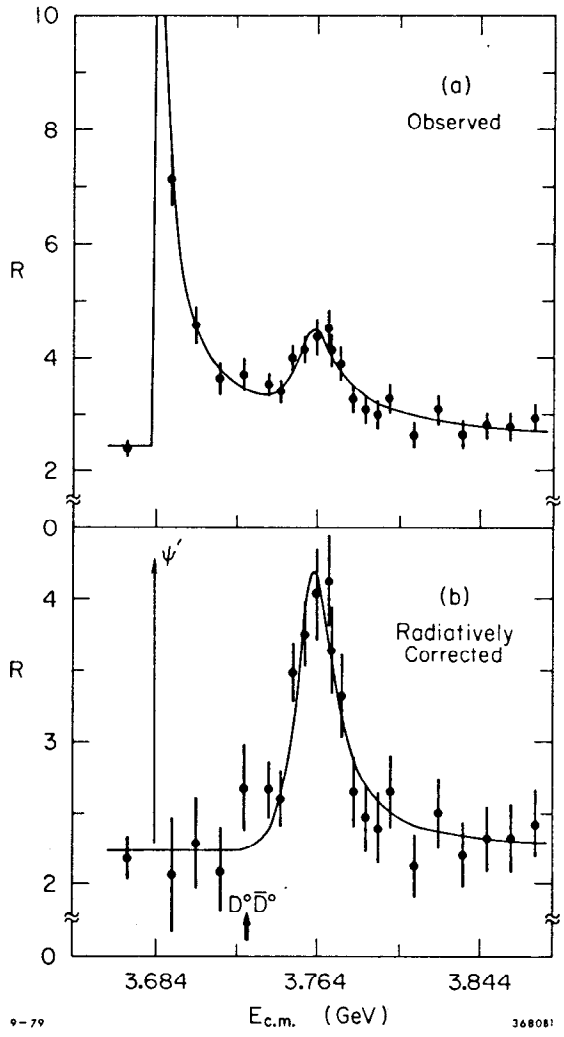

Fig. 16. The ratio of the hadron cross section to the μ-pair cross section in the region of the ψ(3770) resonance for (a) observed and (b) radiatively corrected for the ψ(3096), ψ(3684) and ψ(3771). The curve represents the fit to the data.

TABLE I

Measurements of the $\psi(3770)$ Resonance Parameters

Experiment	Mass MeV/c^2	Γ_{tot} MeV	Γ_{ee} eV	ΔM^* MeV/c^2
DELCO[22]	3770 ± 6	24 ± 5	180 ± 60	86 ± 2[24]
LGW[21]	3772 ± 6	28 ± 5	345 ± 85	88 ± 3
Mark II	3764 ± 5	24 ± 5	276 ± 50	80 ± 2

* ΔM is the mass difference between the $\psi(3684)$ and $\psi(3770)$.

measuring masses relative to the $\psi(3684)$ and this comparison is shown in the last column in Table I. The mass disagreement is now more significant.

The $\psi(3770)$ is typically associated with the $^3D_1$ state of charmonium and the Mark II values for the resonance parameters are in good agreement with the theoretical predictions.[25] In such charmonium models the relatively large leptonic width of the $\psi(3770)$ results from its mixing with the $^3S_1$ state, $\psi(3684)$. We obtain a mixing angle of $(20.3 \pm 2.8)^\circ$.

DECAYS OF CHARMED MESONS

The data presented below was obtained from the fixed energy running at 3.771 GeV, which corresponds to 49,000 hadronic events in the Mark II. From the scan data we measure $\sigma_{D\bar{D}}(3771) = 6.85 \pm 1.2$ nb and further obtain the inclusive $D^\pm$ and $D^\circ(\bar{D}^\circ)$ cross sections by assuming that the $\psi(3770)$ is a resonance of definite isospin (either 0 or 1) and that the decays of the $\psi(3770)$ are saturated by $D\bar{D}$. The assumption concerning isospin leads to the consequence of equal partial widths to the states $D^\circ\bar{D}^\circ$ and D^+D^- up to a phase space factor and the saturation of the decay channels by $D\bar{D}$ is reasonable in light of the narrow width of the nearby $\psi(3684)$. Hence we obtain

$$\sigma_{D^+}(3771) = 5.9 \pm 1.0 \text{ nb}$$

$$\sigma_{D^\circ}(3771) = 7.8 \pm 1.2 \text{ nb} \quad .$$

At the $\psi(3770)$ one is able to exploit the $D\bar{D}$ pair production by using the beam energy and the small D momentum to obtain invariant mass resolution of ~ 3 MeV/c^2. For any combination of particles which are candidates for D meson decay states we require that the energy of those particles be within 50 MeV of the beam energy and calculate the invariant mass using the beam energy (E_b):

$$M = \sqrt{E_b^2 - p^2}$$

where p is the momentum of the particle combination (~280 MeV/c). Figures 17 and 18 show the invariant mass for various $D^o(\bar{D}^o)$ and $D^{\pm}$

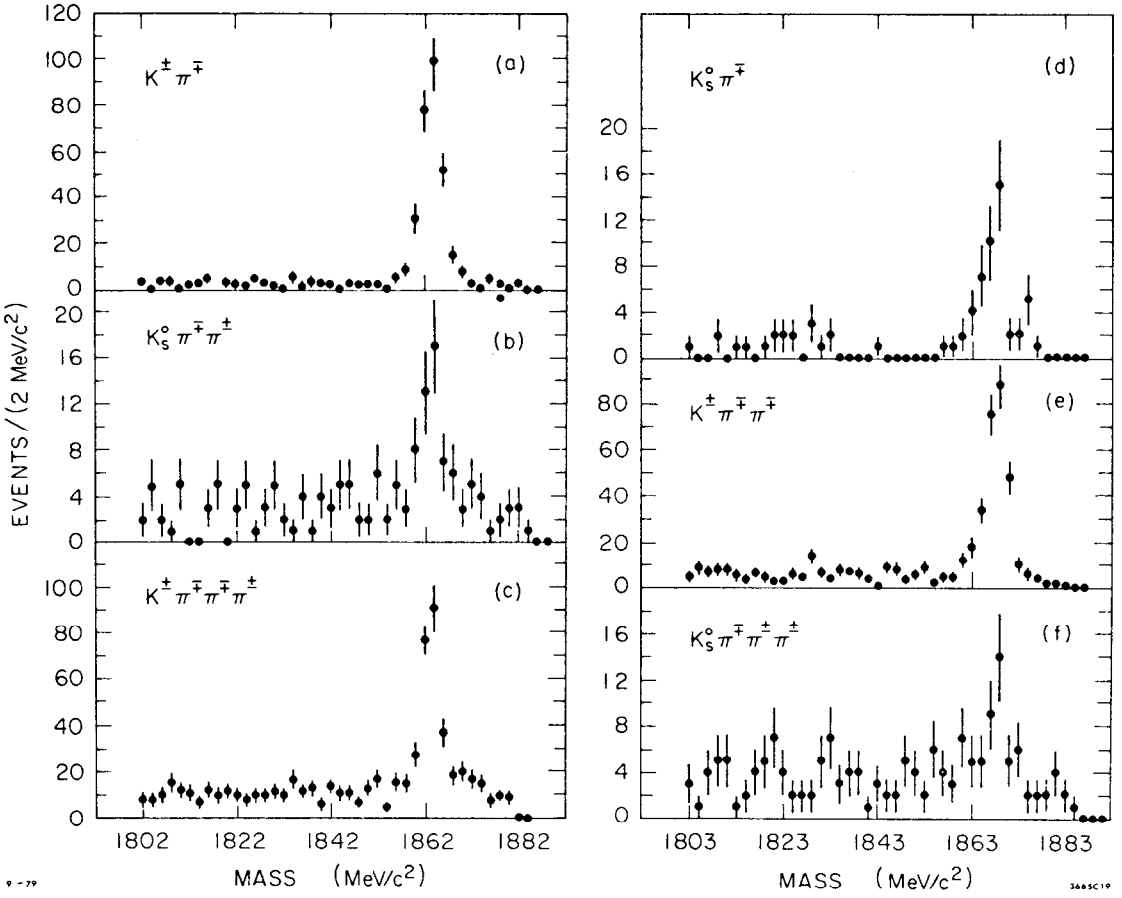

Fig. 17. Invariant mass spectra for various $D^o(\bar{D}^o)$ decay modes (a)-(c) and $D^{\pm}$ decay modes (d)-(f).

decay states. The low level of background in the $D^o \to K^-\pi^+$, $D^o \to K^-\pi^-\pi^+\pi^+$ and $D^+ \to K^-\pi^+\pi^+$ channels is evident and these channels will be used in a later section as clean tags of events containing D's to study inclusive D meson properties. Table II summarizes the results of the D branching fraction study along with a comparison with the results of the LGW experiment.[26] It is interesting to note that the rate for $D^o \to \bar{K}^o\pi^o$ is roughly the same as for $D^o \to K^-\pi^+$ which contradicts the theoretical prediction of color suppression.[27]

In addition to the Cabibbo favored decay channels discussed above, we have observed the Cabibbo suppressed decay modes $D^o \to K^+K^-$ and $D^o \to \pi^+\pi^-$. Figure 19 shows quark diagrams for the Cabibbo favored decay mode as well as the two Cabibbo suppressed modes, and those diagrams reflect the flavor preference for the $c \to s$ coupling over the $c \to d$ coupling. In Fig. 19, θ_A is the familiar Cabibbo angle (θ_c) whereas θ_B can be thought of as the charm analogue of θ_c. Both θ_A

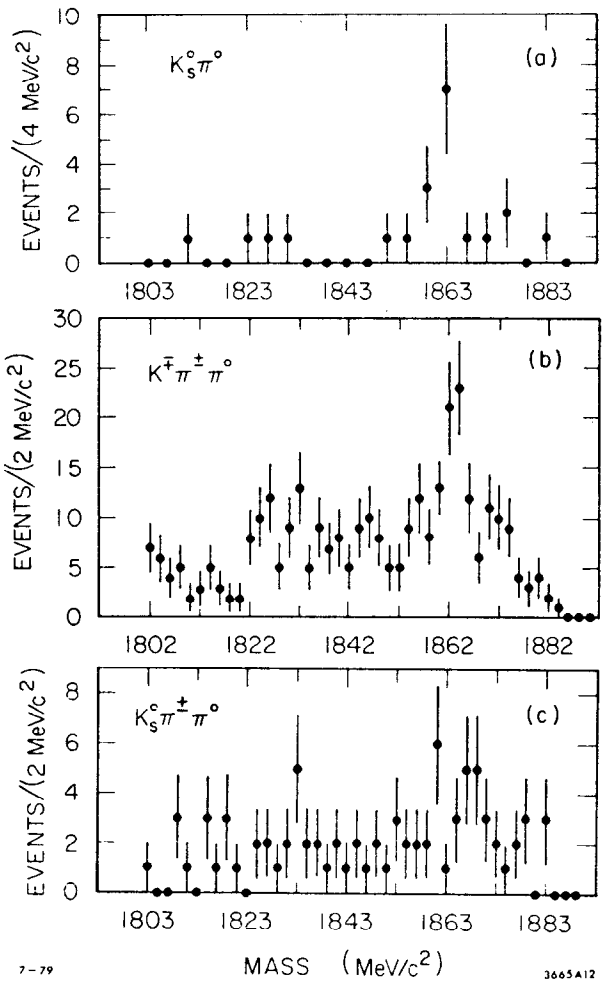

Fig. 18. Invariant mass spectra for the decays (a) $D^0 \to K^0_S\pi^0$, (b) $D^0 \to K^-\pi^+\pi^0$ and (c) $D^+ \to K^0_S\pi^+\pi^0$.

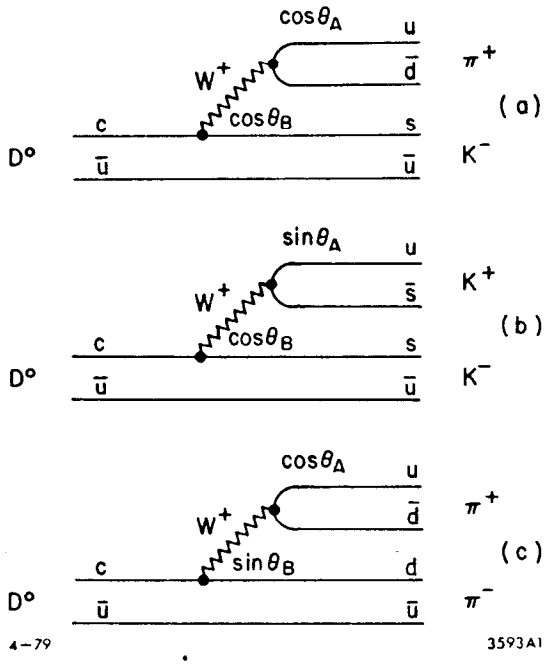

Fig. 19. Quark diagrams for D^0 decays into two charged particles.

TABLE II

D-Meson Branching Ratios

Mode	# Events	ε	BR(%)	Mark I[29] BR(%)
$K^-\pi^+$	271 ± 17	0.436	2.8 ± 0.5	2.2 ± 0.6
$\bar{K}^o\pi^o$	9 ± 3	0.021	2.1 ± 0.9	
$\bar{K}^o\pi^+\pi^-$	39 ± 7	0.064	2.7 ± 0.7	4.0 ± 1.3
$K^-\pi^+\pi^o$	37 ± 9	0.028	6.3 ± 2.2	12.0 ± 6.0
$K^-\pi^+\pi^+\pi^-$	197 ± 16	0.133	6.7 ± 1.4	3.2 ± 1.1
$\pi^+\pi^-$	9 ± 4	0.52	0.09 ± 0.04	
K^+K^-	22 ± 5	0.37	0.31 ± 0.09	
$\bar{K}^o\pi^+$	37 ± 7	0.10	2.1 ± 0.5	1.5 ± 0.6
$K^-\pi^+\pi^+$	251 ± 17	0.29	5.2 ± 1.0	3.9 ± 1.0
$\bar{K}^o\pi^+\pi^o$	9 ± 4	0.004	16.4 ± 9.5	
$\bar{K}^o\pi^+\pi^+\pi^-$	22 ± 7	0.025	5.1 ± 2.0	
$K^-\pi^+\pi^+\pi^+\pi^-$	5 ± 3.5	0.041	< 2.0*	
$\bar{K}^oK^+$	6 ± 3	0.07	0.5 ± 0.27	

* 90% confidence limit.

and θ_B can be measured via the relations

$$\tan^2\theta_A = \frac{\Gamma(D^o \to K^+K^-)}{\Gamma(D^o \to K^-\pi^+)} \quad ; \quad \tan^2\theta_B = \frac{\Gamma(D^o \to \pi^+\pi^-)}{\Gamma(D^o \to K^-\pi^+)} \ .$$

Under the assumption $\theta_A = \theta_B$ and SU(3) invariance, one can predict $\tan^2\theta_A = \tan^2\theta_B = \tan^2\theta_C = 0.05$. Because of phase space considerations the rate for the $D^o \to \pi^+\pi^-$ mode is raised by 7% and the rate for the $D^o \to K^+K^-$ mode is lowered by 8%.

In the analysis of the three two body modes mentioned above we require that the pair momentum (p_D) be within 30 MeV/c of the expected momentum (288 MeV/c). The two body invariant masses for the three mass assignments are plotted in Fig. 20. One sees a prominent peak at the D_o mass (1863 MeV/c^2) in the $K^-\pi^+$ mode, a clear signal in the K^+K^- mode and a statistically significant excess of events in the $\pi^+\pi^-$ mode. The peaks in Figs. 20(a) and 20(b) which appear at ~±120 MeV/c^2 relative to the D mass arise from the decay $D^o \to K^-\pi^+$ in which either a K or a π are misidentified by TOF. The data in Fig. 20 is fit using the technique of maximum likelihood. Background distributions shown in Fig. 20 are obtained from sidebands in the p_D plot.

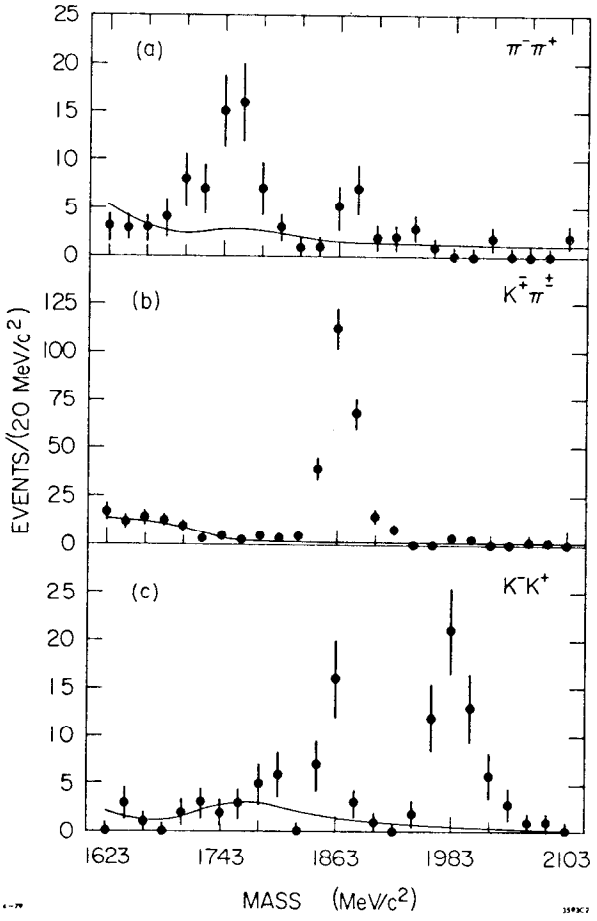

The results of the fit are 235 ± 16 $K^{\pm}\pi^{\mp}$ events, 22 ± 5 K^+K^- events and 9 ± 3.9 $\pi^+\pi^-$ events. Accounting for the relative efficiencies gives $\Gamma(D^o \to K^+K^-)/\Gamma(D^o \to K^-\pi^+) = 0.113 \pm 0.03$ and $\Gamma(D^o \to \pi^+\pi^-)/\Gamma(D^o \to K^-\pi^+) = 0.033 \pm 0.015$. The errors quoted include systematic effects the most prominent of which is the background estimate used for the fit. The results show that Cabibbo suppressed D decays exist and that they have roughly the expected magnitude.

Fig. 20. Invariant mass of two particle combinations with momenta within 30 MeV/c of the expected D^o momentum.

INCLUSIVE STUDIES OF D-MESON DECAYS

As we mentioned before, the relatively background-free channels $D^o \to K^-\pi^+$, $D^o \to K^-\pi^+\pi^-\pi^+$ and $D^+ \to K^-\pi^+\pi^+$ are used for inclusive studies. The observed D channel serves as a clean tag for $D\bar{D}$ production and we look to see what is produced in association with the tag. For these inclusive studies a sample of events comprising 283 $K^-\pi^+$ decays (with 17 ± 2 background), 211 $K^-\pi^+\pi^-\pi^+$ decays (with 31 ± 3 background) and 290 $K^-\pi^+\pi^+$ decays (with 33 ± 2 background) are used.

Figure 21(a) shows the observed charge multiplicity opposite the tagged events. These spectra have been corrected for the background contributions shown shaded in the plot. The distributions are not corrected for the $K_s \to \pi^+\pi^-$ decay which enters into the spectra in Fig. 21 as two charged particles. Using a Monte Carlo simulation program one obtains a matrix which relates the probability of observing j charged particles when i were produced. This matrix is used to "unfold" the produced charged multiplicity, the results of which are shown in Fig. 21(b). The average multiplicities are:

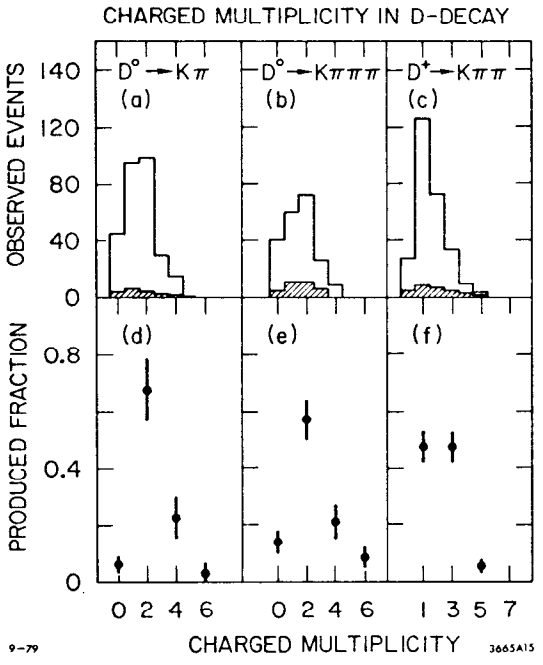

Fig. 21. The observed (a)-(c) and produced (d)-(f) charged multiplicity distributions obtained using the channels $D^o \to K^-\pi^+$, $D^o \to K^-\pi^+\pi^-\pi^+$ and $D^+ \to K^-\pi^+\pi^+$ as tags.

$$\langle n_{ch} \rangle_{D^o} = 2.46 \pm 0.14$$

$$\langle n_{ch} \rangle_{D^+} = 2.16 \pm 0.16 \ .$$

The mean charged multiplicities are similar in magnitude because the D^o decays primarily into two charged particles while the D^+ decays roughly equally into one and three charged particles. These results agree well with a previous measurement of $\langle n_{ch} \rangle = 2.3 \pm 0.3$ by the LGW group[29] and are lower than the typical predictions of statistical models.[30]

Because of the favored flavor change $c \to s$ involved in D decays, one expects to see a kaon in most D decays. The tagged events have been used to measure the kaon content in D decay. As usual charged kaons are identified from TOF and neutral kaons via the decay $K_S \to \pi^+\pi^-$. Table III summarizes the results of this study. The backgrounds for charged kaons come from TOF misidentifications and for neutral kaons from random $\pi^+\pi^-$ pairs whose mass is consistent with a K_S. From Table III we can conclude that the Cabibbo suppressed decays ($\bar{D} \to K^+$) are seen at the expected rate. The rate for $D^+ \to K^-$

TABLE III

Kaon Content in D Decays

Decay Mode	# Tags	# Kaons	Background	BR(%)
$D^o \to K^-$	476 ± 23	111	5.1 ± 1.2	56 ± 5.6
$\to K^+$		20	5.8 ± 1.3	7.9 ± 2.6
$\to K^o$		15	5.1 ± 0.5	20.3 ± 8.5
$D^+ \to K^-$	257 ± 18	21	2.2 ± 0.7	17.2 ± 4.1
$\to K^+$		11	4.5 ± 1.6	5.6 ± 2.9
$\to K^o$		13	3.5 ± 0.4	44.0 ± 15.0

is suprisingly low. However, this measurement is in good agreement with $(10 \pm 7)\%$ obtained by LGW.[29] Although the errors are large, particularly for the $D \to K^o$ rates, the inclusive fraction of both D^o and D^+ into kaons are lower than naive expectations.

We have studied semi-leptonic D decays using the electron content in tagged events. Here we must distinguish between "right sign" and "wrong sign" electrons - the "wrong sign" electron having the opposite sign of the kaon observed in the tagged D. The data are summarized in Table IV. The excess (observed events above background) of "right sign" events are corrected using the excess of "wrong sign" events in order to obtain the true branching fractions. We note that $B(D^+ \to e^+)$ is approximately three times as large as $B(D^o \to e^+)$. If we assume that the D^+ and D^o have the same semi-leptonic widths we obtain

$$\frac{\Gamma(D^o \to \text{all})}{\Gamma(D^+ \to \text{all})} = \frac{B(D^+ \to e^+)}{B(D^o \to e^+)} = \frac{\tau^+}{\tau^o}$$

Hence measurement of the ratio of the leptonic branching fractions for D^+ and D^o measures their relative lifetimes. Using the data in Table IV and a maximum likelihood method which incorporates the (Poisson) statistics of the observed events and the subtractions we obtain

$$\frac{\tau^+}{\tau^o} = 3.08 \begin{matrix} + 4.1 \\ - 1.33 \end{matrix} .$$

DELCO has reported a similar trend in the relative lifetimes of the D^+ and D^o.[31] Correcting for phase space effects we also obtain

$$B(D \to e^+) = (9.8 \pm 3.0)\% .$$

TABLE IV

Semi-Leptonic Decays of D^+ and D^o

Decay Mode	# Tags	# Electrons	Background	BR(%)
$D^+ \to e^+$	295 ± 18	38	15 ± 1	15.8 ± 5.3
$\to e$		4	3.9 ± 0.5	
$D^o \to e^+$	480 ± 23	36	19 ± 1	5.2 ± 3.3
$\to e$		19	12 ± 1	

CONCLUSIONS

The Mark II is able to make valuable contributions to the understanding of a broad range of physics topics. Data from the study of τ hadronic decays agree well with the theoretical predictions. The mode $\tau \to \rho\nu$ supports the CVC hypothesis and the decay $\tau \to K^*(890)\nu$ is evidence of the presence of a Cabibbo suppressed vector current in τ decays. The studies of D decay properties are in may cases statistics limited but there are some significant disagreements with the standard theoretical lore. In particular color suppression is not supported by the data, the fraction of both D^o and D^+ decaying to a kaon seems low, the D^o and D^+ have lifetimes differing by about a factor of 3 and there are still a large fraction of D decay modes unaccounted for. Cabibbo suppressed D decays have been observed at approximately the expected rate. A direct photon signal has been observed at the ψ, and the rate for these direct photons agrees well with the prediction of first order QCD calculations. However the shape of the direct photon momentum distribution is in poor agreement with this QCD prediction and better theoretical input is needed. Clear evidence for the charmed baryon Λ_c^+ has been seen for the first time in e^+e^- interactions. The Λ_c^+ is seen decaying into at least two decay channels and an absolute branching fraction is obtained for the decay $\Lambda_c^+ \to pK^-\pi^+$. Unfortunately it appears as though we have insufficient data to obtain a clear understanding of the charmed baryon spectroscopy and this task will have to be left to future experiments.

REFERENCES

1. Members of the SLAC-LBL collaboration: G. S. Abrams, M. S. Alam, C. A. Blocker, A. M. Boyarski, M. Breidenbach, C. H. Broll, D. L. Burke, W. C. Carithers, W. Chinowsky, M. W. Coles, S. Cooper, B. Couchman, W. E. Dieterle, J. B. Dillon, J. Dorenbosch, J. M. Dorfan, M. W. Eaton, G. J. Feldman, H. G. Fischer, M. E. B. Franklin, G. Gidal, G. Goldhaber, G. Hanson, K. G. Hayes, T. Himel, D. G. Hitlin, R. J. Hollebeek, W. R. Innes, J. A. Jaros, P. Jenni, A. D. Johnson, J. A. Kadyk, A. J. Lankford, R. R. Larsen, D. Lüke, V. Lüth, J. F. Martin, R. E. Millikan, M. E. Nelson, C. Y. Pang, J. F. Patrick, M. L. Perl, B. Richter, J. J. Russell, D. L. Scharre, R. H. Schindler, R. F. Schwitters, S. R. Shannon, J. L. Siegrist, J. Strait, H. Taureg, V. I. Telnov, M. Tonutti, G. H. Trilling, E. N. Vella, R. A. Vidal, I. Videau, J. M. Weiss, and H. Zaccone.
2. G. S. Abrams et al., Phys. Rev. Lett. 43, 477 (1979).
3. W. Davies-White et al., Nucl. Instrum. Methods 160, 227 (1979).
4. G. S. Abrams et al., to be published in IEEE Trans. on Nucl. Sci. NS-27, 1 (Feb. 1980); G. S. Abrams et al., IEEE Trans. on Nucl. Sci. NS-25, 1, 309 (1978).
5. EGS, Electromagnetic Shower Program, R. L. Ford and W. R. Nelson, SLAC-Report 210 (1978).

6. See for instance G. Feldman, Proceedings of the 19th International Conference on High Energy Physics, Tokyo, 1978, p. 777.

7. W. Bacino et al., Phys. Rev. Lett. 42, 749 (1979).

8. The notation $\tau^- \to \rho^- \nu_\tau$, $\tau^- \to \ell^- \nu_\tau \bar{\nu}_e$ and $\tau^- \to \pi^- \nu_\tau$ imply also the charge conjugate reactions.

9. G. S. Abrams et al., Phys. Rev. Lett. 43, 1555 (1979).

10. F. J. Gilman and D. H. Miller, Phys. Rev. D17, 1846 (1978).

11. R. Brandelik et al., Z. Phys. C1, 233 (1979).

12. Y. S. Tsai, Phys. Rev. D4, 2821 (1971).

13. See for instance S. J. Brodsky et al., Phys. Lett. 73B, 203 (1978).

14. This value of α_s is calculated from the ratio of the leptonic to the hadronic width of the ψ [see T. Appelquist and H. D. Politzer, Phys. Rev. Lett. 34, 43 (1975)]. The predicted direct photon contirubtion is included in the $\Gamma_{tot}(\psi)$ used in the calculation.

15. G. S. Abrams et al., submitted to Phys. Rev. Lett. (1979), SLAC-PUB-2406 and LBL-9855 (1979).

16. R. Brandelik et al., Nucl. Phys. B148, 189 (1979).

17. M. Piccolo et al., Phys. Rev. Lett. 39, 1503 (1977).

18. E. G. Cazzoli et al., Phys. Rev. Lett. 34, 882 (1976); A. M. Cnops et al., Phys. Rev. Lett. 42, 197 (1979); C. Baltay et al., Phys. Rev. Lett. 42, 1721 (1979); C. Angelini et al., Phys. Lett. 80B, 428 (1979). Contributions to the EPS Conference on High Energy Physics, Geneva 1979; D. Drijard et al., CERN-EP preprint (1979); K. L. Giboni et al., CERN-EP preprint (1979); P. Schlein et al., UCLA preprint (1979).

19. An upper limit of 0.5 nb (90% C.L.) on the production of charmed baryons in association with a charmed meson, $\bar{D}^0$ or D^-, had been obtained from a handscan of all events with a measured decay $D^0 \to K\pi$.

20. This value is somewhat model dependent. The quoted value was estimated from our measurements of $\Delta R(p + \bar{p})$ and $\Delta R(\Lambda + \bar{\Lambda})$ and a simple isospin statistical model.

21. P. A. Rapidis et al., Phys. Rev. Lett. 39, 526 (1977).

22. W. Bacino et al., Phys. Rev. Lett. 40, 671 (1978).

23. Cool and Marshak, Advances in Particle Physics, Vol. 2, p. 193 (1968).

24. Private communication, Walt Bacino, UCLA.

25. E. Eichten et al., Phys. Rev. D17, 3090 (1978); T. Appelquist et al., Ann. Rev. Nucl. Sci. 29, 387 (1978).

26. I. Peruzzi et al., Phys. Rev. Lett. 39, 1301 (1977).

27. D. Fakirov, B. Stech, Nucl. Phys. B133, 315 (1978); N. Cabibbo and L. Maiani, Phys. Lett. 73B, 418 (1978).

28. G. S. Abrams et al., Phys. Rev. Lett. 43, 481 (1979).

29. V. Vuillemin et al., Phys. Rev. Lett. 44, 1149 (1978).

30. C. Quigg and J. L. Rosner, Phys. Rev. D17, 239 (1978).

31. J. Kirkby, 1979 International Symposium on Lepton and Photon Interactions at High Energy, Batavia, August 23-29, 1979; SLAC-PUB-2419.